Optimization of the Rheological Properties of Fumed-Silica-Based Supporting Baths for Embedded Printing and Reduction of the Effect of Crevasse Formation

Vera, Grace; Tisato, Silvio; Nekoonam, Niloofar; Shakeel, Ahmad; Garfias, Stephanie; Helmer, Dorothea

DOI
10.1002/admt.202400533

Publication date
2024

Document Version
Final published version

Published in
Advanced Materials Technologies

ADVANCED MATERIALS TECHNOLOGIES
www.advmattechnol.de

Optimization of the Rheological Properties of Fumed-Silica-Based Supporting Baths for Embedded Printing and Reduction of the Effect of Crevasse Formation

*Grace Vera, Silvio Tisato, Niloofar Nekoonam, Ahmad Shakeel, Stephanie Garfias, and Dorothea Helmer**

In embedded 3D printing, the supporting gel must provide the right rheological properties to keep the ink in place. It has previously been shown that a strong and stable 3D network can be formed by particle–particle interactions of hydrophobic fumed silicas suspended in a polar solvent. Here, the rheological properties of fumed silica gels in polyethylene glycol (PEG) are investigated. The recovery properties like storage modulus, yield stress, and recovery time of the gels made of fumed silica with alkyl-chains of different lengths are studied. A very fast recovery time (0.2 s) is achieved by increasing the length of the alkyl chains on the silica surface, leading to embedded printing results with high shape accuracy. However, with the engineered supporting gel, the formation of crevasses affects the shape of the filament. Previous approaches to reduce crevasse formation include the introduction of liquid fillers to avoid such distortions, which, however, prevents the reuse of the gels and leads to increasing waste production in embedded printing. Here, it is shown that by adjusting the rheology of the inks to fit the rheology of the supporting gel, high-shape accuracy prints with ideally round-shaped filaments can be achieved without the need for liquid fillers.

1. Introduction

In embedded 3D printing, a needle extrudes a liquid ink into a supporting bath layer by layer to build a 3D structure without the need for the printing of additional material supports, which saves material and printing time.[1,2] With embedded printing, various materials have been printed, including acrylates,[3] silicones,[4] or ceramics.[5] The rheological behavior of the inks plays a crucial role in the success of the embedded print. Inks must exhibit shear thinning behavior to allow the extrusion through a thin needle, and the interfacial tension between the ink and supporting bath must be low to assure continuous filaments and prevent them to break up into droplets.[6–9] However, the rheological properties of the supporting bath are equally important and more complex. The supporting bath plays a crucial role in the printing, as it ensures the precise deposition of the ink. To achieve this, the supporting bath has to show several unique properties. These are a) solid-like behavior to hold the printed ink in place, b) shear thinning and yielding at a low shear rate to guarantee immediate local fluidizing behavior around the needle, thus allowing the deposition of the filament ink, c) a fast recovery time to trap the filament and keep its shape without deformation.[10] Thus, in terms of rheological properties, the bath must a) show soft gel-like behavior with a sufficiently high storage modulus G', which must be strong enough to hold the printed 3D structure in place.[11] As printing and curing times vary, material properties must be stable over time, and G' must be dominant over G'' and time-independent at rest, indicating steady gel-like behavior. Several authors have reported storage moduli for supporting baths in the range of 10^1–10^3 Pa,[6,11–13] in which 3D printed inks retained their shape for an extended time (6 months).[1] To achieve b) the bath must be shear thinning and yielding, i.e., be a yield stress fluid (YSF), which enables the in situ deposition and support of the filament ink.[14,15] Earlier studies have reported a large range of values for the required yield stress. Supporting baths with low yield stress, such as ≈10 Pa can be sufficient for supporting properties.[4,6,16] An important property to achieve c) is the quick transition from

G. Vera, S. Tisato, N. Nekoonam, S. Garfias, D. Helmer
Freiburg Materials Research Center (FMF)
Albert-Ludwigs-University Freiburg
79104 Freiburg im Breisgau, Germany
E-mail: dorothea.helmer@imtek.uni-freiburg.de

N. Nekoonam, D. Helmer
Laboratory of Process Technology
Department of Microsystems Engineering (IMTEK)
Albert-Ludwigs University Freiburg
79110 Freiburg im Breisgau, Germany

A. Shakeel
Department of Aerospace Structures and Materials
Delft University of Technology
Delft 2629 HS, Netherlands

D. Helmer
Freiburg Center of Interactive Materials and Bioinspired Technologies (FIT)
University of Freiburg
79110 Freiburg im Breisgau, Germany

The ORCID identification number(s) for the author(s) of this article can be found under https://doi.org/10.1002/admt.202400533

DOI: 10.1002/admt.202400533

liquid to solid after removal of the shear rate applied by the movement of the needle.[17] This rapid recovery time of the viscoelastic properties of the supporting bath permits to trap the printed filaments in place and keeps its shape without deformation.[10] Suitable recovery time for embedded 3D printing has been reported to be in the range of <1 s.[7] Besides these fundamental requirements, there are also other influences on the accuracy of the prints. The crevasses (air pockets) forming behind the needle can only collapse if the baths yield stress is lower than the hydrostatic pressure at the depth of the print.[1] If the crevasses do not collapse, the deposited inks can flow into these pockets, causing a deformation of the printed ink path. One approach to prevent this is the use of Newtonian liquid fillers that are deposited on top of the supporting batch and readily flow into the created air pockets.[8] However, this approach can be challenging as it introduces a third material into the process, which needs to be adjusted to fit the print requirements and prevents the re-use of the supporting baths because of the effect of mixing the bath and the Newtonian filler.

Several different supporting materials for embedded printing have previously been reported. The materials consist of solid particles suspended in a suitable solvent and are classified into two types by the particle/solvent interactions, which are either repulsive or attractive. Granular materials like Carbopol[3,9,18] are examples of repulsion-dominated interaction, and particulate gels like fumed silica in organic solvents belong to the attraction-dominated materials.[2,19,20] The rheological properties of gels made from fumed silica have been widely studied with different particle sizes in different solvents.[21–24] The evidence suggests the formation of a solvation layer when fumed silica is suspended in a solvent with similar polarity – this induces the formation of a stable sol instead of a gel.[25–27] To achieve the formation of a gel and to control the rheological properties of these gels, fumed silica must be suspended in a suitable solvent in which the network is governed primarily by particle/particle interactions. The rheology of fumed silica based supporting baths can be readily engineered. Moriana et al. investigated the effect of the size of fumed silica particles on the shear thinning and shear thickening behavior in polyethylene glycol (PEG) and polypropylene glycol (PPG). They found that the optimal concentration of fumed silica in the solvent depends on the particle size, and the shear thickening effect increases with larger particle size.[28] Alaee et al. show similar findings, suggesting that a reduction of the particle size or increasing the hydrophobicity of silica in PEG causes the formation of gels with higher elastic modulus.[29] In a study conducted by Raghavan et al., the surface chemistry of fumed silica with different nonpolar alkyl chains showed an effect on the solid-like behavior and yield stresses:[30] The authors reported stronger storage modulus for fumed silica with longer tethered chains due to the higher surface coverage, and the ready formation of gels in polar organic media. The careful choice of fumed silica and solvent allows for the control of the rheological properties of the materials. With a carefully adjusted supporting bath rheology, optimal embedded printing results can be achieved in terms of structure fidelity and support.

Here, we show the rheological properties of supporting baths created from different hydrophobic fumed silica in polyethylene glycol. We provide an analysis focused on the recovery of the viscoelastic properties of fumed silica with alkyl chains of different lengths. To quantify the effect of the chain length on the rapid deformation, recovery, and stability of the supporting bath, we investigated the rheological properties under dynamic and steady-state shearing. We find that gels formed from fumed silica with longer hydrophobic chains possess higher yield stress and also require less time to recover the gel state. These properties ensure a high shape-accuracy in embedded printing. However, the increased yield stress also fosters the formation of crevasses, thus deforming the printed ink filaments due to the ink flowing into the crevasses. We show that this effect can be mitigated by engineering the printing ink to achieve high viscosity, shear-thinning materials. The combination of the engineered supporting baths and the engineered inks ensures high accuracy embedded printing without the need for liquid fillers.

2. Experimental Section

2.1. Materials

Hydrophobic fumed silica Aerosil R974, R812, R805 for the supporting bath preparation, and R816 for the ink modification were supplied by A.+E. Fischer–Chemie GmbH & Co. KG. A schematic representation of the surface chemical structures of R974, R812, and R805 are shown in **Figure 1a**. Polyethylene glycol 200 (PEG) (60 mPa s) and 2,2-Dimethoxy-2-phenylacetophenone were purchased from Sigma–Aldrich. Fluorolink MD 700 (a perfluoropolyether (PFPE) dimethacrylate (MA)) was supplied by Acota. All the chemicals were used as received without further treatment.

2.2. Preparation of Supporting Baths and Modified Inks

Supporting baths were prepared as follows: Fumed silica R974, R812, and R805 were homogenously dispersed at 10% (w/v) in polyethylene glycol using a speed mixer (DAC 150.1 FVZ, Hauschild) at 3500 rpm for 2.5 min. Modified inks were prepared as follows: Fluorolink MD 700 was modified with 5%(w/v) and 10% (w/v) of fumed silica R816 to increase the viscosity. 0.5% (wt.) of 2,2-Dimethoxy-2-phenylacetophenone was used to polymerize the ink.

2.3. UV–vis Transmittance of the Supporting Baths

The transmittance of UV–vis spectra of the supporting baths was recorded using UV–vis spectrophotometer Evolution 201 (ThermoScientific, Germany) using polystyrene UV cuvettes. The measured wavelength was recorded from 350 to 750 nm. Polyethylene glycol (PEG) was used as blank.

2.4. Rheological Characterization

Rheological properties of the gels were tested using a Haake Mars II rheometer (Thermo Fisher Scientific) using a titanium serrated 35 mm parallel upper and lower plate with a gap of 0.5 mm. A serrated plate was used to avoid wall slip effect. To characterize the soft solid-like behavior at rest, oscillatory frequency

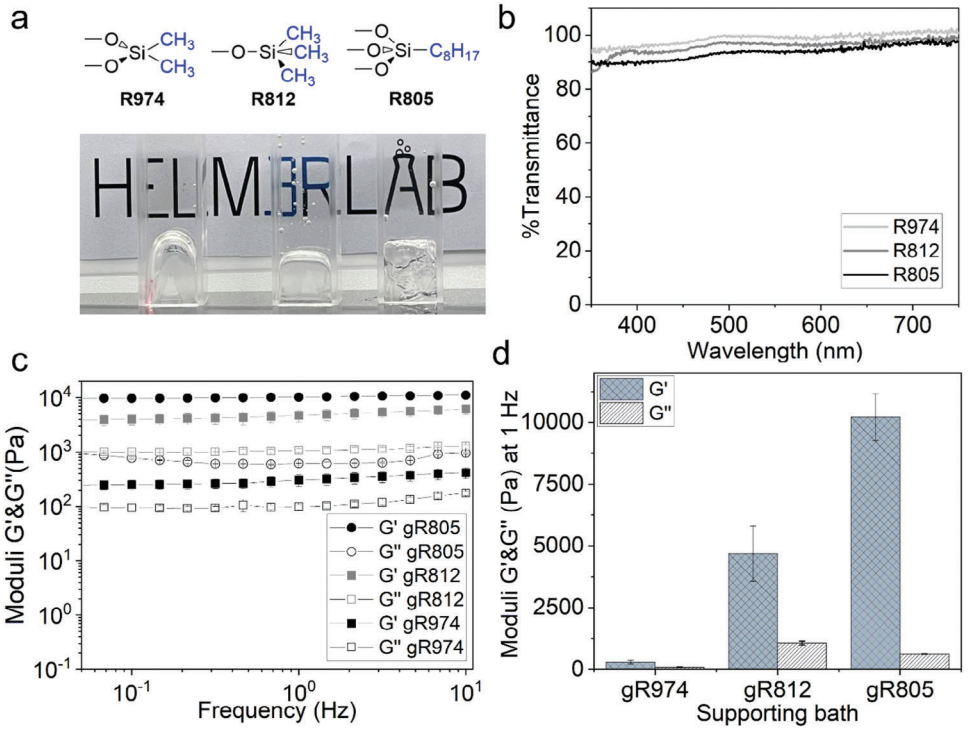

Figure 1. Gel-like properties of different types of hydrophobic fumed silicas R974, R812, and R805 in polyethylene glycol (PEG 200) at 10%w/v. a) Hydrophobic fumed silicas with methylsilyl-, dimethylsilyl-, and octylsilyl-sidechains for R974, R812, and R805 were used to create transparent gels gR974, gR812 and gR805. Note that the containers are upside down to emphasize the gel-like character of the materials. b) UV–vis Spectra of the gels showing high optical transparency between 350 nm and 750 nm. c) Proof of gel-like behavior with G' dominating over G'' at all frequencies between 0,05 Hz and 10 Hz for each transparent gel. d) Elastic modulus for each gel derived from (c). Elastic modulus in the silica/PEG gels increase from R974 to R812 to R805. The storage modulus values are 311, 5483, and 10267 Pa for gR974, gR812, and gR805, respectively.

sweep test at low frequencies from 10 to 0.01 Hz and deformation within the linear viscoelastic behavior of 0.002% was performed. Shear thinning behavior and yield stress were analyzed in steady state shearing mode by control shear rate from 300 to 0.001 s^{-1}. The recovery of storage modulus time was obtained by oscillatory time sweep test by applying 1% strain during 120 s and immediately dropped to 0.001% strain both values belong to the non-linear and linear viscoelastic region, respectively. All measurements were performed at a temperature of 23 °C.

2.5. Embedded 3D Printing

A commercial linear delta printer (Kossel Linear, Anycubic) was modified by substituting the effector and hotend assembly with a custom 3D printed syringe pump integrated into the effector. The ink was loaded in 1 mL syringes (Injekt-F, B-Braun) equipped with 0.4 mm internal diameter blunt-tip stainless steel needles (Vieweg Gmbh). The print jobs were generated by slicing 3D models created in AutoDesk Inventor with SuperSlicer. GCode for complex freeform parts was generated via a custom Python script inspired by FullControlGcode.[31] Printing speed was set to 15 mm s^{-1}, and extrusion width and height were set according to the dimension of the needle to 0.4 and 0.4 mm, respectively, for the filaments and adjusted to 0.3 and 0.3 mm, respectively, for the 3D prints to ensure a better merging between the layers. After the print job was completed, the vessel containing the support matrix and printed ink was placed in a UV Curing Chamber (XYZ Printing) and exposed to 365–405 nm UV light for 6 min to cure.

2.6. Characterization of Embedded Filaments and Prints

Scanning electron microscopy (SEM) was used to analyze the roundness of the filament. Photographs were taken with a color camera (VCXU-15C, Baumer) and videos were recorded with a monochrome camera (VCXU-15M, Baumer) at a frame rate of 225 fps.

3. Results and Discussion

For embedded printing, suitable supporting baths have to be designed to ensure printing with high shape-accuracy. Fumed silica is a readily available rheological modifier and can be used to design novel supporting baths by the right combination of particles and solvents. In this study, different rheological properties for supporting bath were engineered using fumed silica particles Aerosil R974, Aerosil R812, and Aerosil R805. The physicochemical properties of the fumed silica are shown in **Table 1**: The fumed silicas are functionalized with different alkyl chain length, which correspond to dimethylsilyl, trimethylsilyl, and octylsilyl (R974, R812, R805).[32] Silica particle sizes vary between 7 nm

Table 1. Physico-chemical properties of fumed silica.[21,33,34]

Fumed silica	Aerosil R974	Aerosil R812	Aerosil R805
Alkyl chain	Dimethylsilyl	trimethylsilyl	octysilyl
Surface alkyl chain length	R974 < R812 < R805		
Particle size [nm]	12	7	12
Surface area [m^2 g^{-1}]	170 ± 20	260 ± 30	150 ± 25
Refractive index	1.460	1.460	1.460
Remaining silanol group density 1 nm^{-2}	0.39	0.44	1.66

(R812) and 12 nm (R974 and R805). As expected, the smaller sized particles of R812 lead to a higher surface area of 260 m^2 g^{-1} than the surface area of the 12 nm samples, which are comparable at 150–170 m^2 g^{-1}, respectively. To achieve the formation of a gel, the particles have to be incorporated into a solvent that facilitates particle/particle interactions resulting in network formation and a higher elastic modulus than gels that also show particle/solvent interactions.[27] The particle size as well as the particle functionalization regarding density, chain conformation and length play a role for the rheological properties of gels. Polyethylene glycol (PEG) was chosen as a solvent due to the mismatch of its polar character to the non-polar surface chemistry of the fumed silica and its matching refractive index of 1.46. For embedded printing, a soft gel with sufficient storage modulus G' is required to hold the extruded ink in place and to prevent the sagging of the printed shape. To test the formation of gels, the fumed silicas from Table 1, with different surface modifications (see Figure 1a) were dispersed in PEG at 10% (w/v). The formation of transparent gels was observed, see Figure 1a,b. From here on, the 10% gels are denoted as gR974, gR812, and gR805 by the type of silica they contain.

Dynamic rheology experiments were performed to test the soft gel-like behavior of the gels. Experiments were conducted to ensure a strain amplitude within the linear viscoelastic region (see Figure S1, Supporting Information). The dynamic rheological responses are presented in Figure 1c. The data shows gel-like behavior for the three samples, gR974, gR812, and gR805, as the elastic modulus (G′) remains constant and dominates over the viscous modulus (G′′) independently of the frequency.[35] A significant increase of the elastic modulus (G′) is observed for gR974, gR812, and gR805, respectively with 311, 5483, and 10267 Pa (at frequency 0.1 Hz) for gR974, gR812, and gR805, respectively (Figure 1d). The strongest network formation is therefore observed with the longest alkyl sidechains of R805. The long sidechains can more easily get into contact and interact with another to form a strong network.

In embedded printing, the movement of the needle through the supporting bath is key for depositing the liquid ink. The formed gels require a network structure that can be momentarily destroyed by applied shear stress or strain to reach the liquid behavior. This transition from solid to liquid behavior is possible when enough deformation is applied to overcome the yield stress of the fluid. In embedded 3D printing, overcoming the yield stress at the relatively low shear rate applied by the movement of the needle, is necessary. The shear rate exerted by the needle can be approximated by the printing speed divided by the needle thickness.[36] For this work we used 15 mm s^{-1} of printing speed and a needle of 700 µm outer diameter, which corresponds to a shear rate of 21 s^{-1}. Next to overcome the yield stress, shear thinning behavior at these low shear rates allows for the deposition of the liquid ink filament while the yield stress holds the deposited filament in place. The prepared fumed silica gels were tested for yield stress behavior (**Figure 2a**). Herschel–Buckley's[11] model was used to fit the flow curves and determine the yield stress. According to the Herschel–Buckley fitting, the yield stress is 10 Pa, 37 Pa and 248 Pa for gR974, gR812, and gR805, respectively. As also observed for the elastic modulus, the highest yield stress is observed in gel R805, which is likely the result of the interactions between the longer alky-chains of the fumed silica, which provide more sites for van der Waals interactions. Figure 2a also shows that the yield stress is overcome at relatively low shear rates for all types of fumed silicas. The low shear rates required to destroy the network indicates that the interactions between the fumed silica correspond to physical bonding. This weak interaction is expected, specially from purely alkyl-type chains. For the shear thinning test, shear rates in the range of the shear rates exerted by the needle (21 s^{-1}) were chosen, as the shearing by the needle needs to ensure the change from solid-like to liquid-like behavior in the gel. A viscosity drop from 10^8 to 10^3 mPa s when increasing the shear rate from 10^{-2} to 10^2 s^{-1} was observed (Figure 2b). The increase of the yield stress also causes the persistence of crevasses in the wake of the needle (Figure 2d). When the hydrostatic pressure at the bottom of the crevasse exceeds the yield stress, the crevasse collapses,[1,19] otherwise, it retains a final size in the range of

$$h = \frac{\sigma_y}{\rho * g} \tag{1}$$

where h is crevasse height, σ_y is the yield stress, and ρ is density and g gravity. With an estimated density of 1,2 g cm^{-3} of the gels, the final size of the crevasse would be in the range of 0.8 mm for gR974, 3 mm for gR812 and 21 mm for gR805 (if the needle was lowered below the point, the crevasses collapse). An experimental print was conducted to analyze the crevasse formation in the gels. For the very low yield stress of gR974, all crevasses readily collapse, and the remaining crevasses are too small to observe (Figure 2d,i), while for increased yield stresses, the crevasses persist with lower (gR812, Figure 2d,ii) and higher height (gR805, Figure 2d,iii). Thus, the data confirms the formation and predicted size of the crevasses. When crevasses form, the deposited ink may flow into the space of these air pockets, causing a deformation of the filament structure from the ideal round shape. Fluorinated acrylate ink Fluorolink MD 700 was chosen due to its

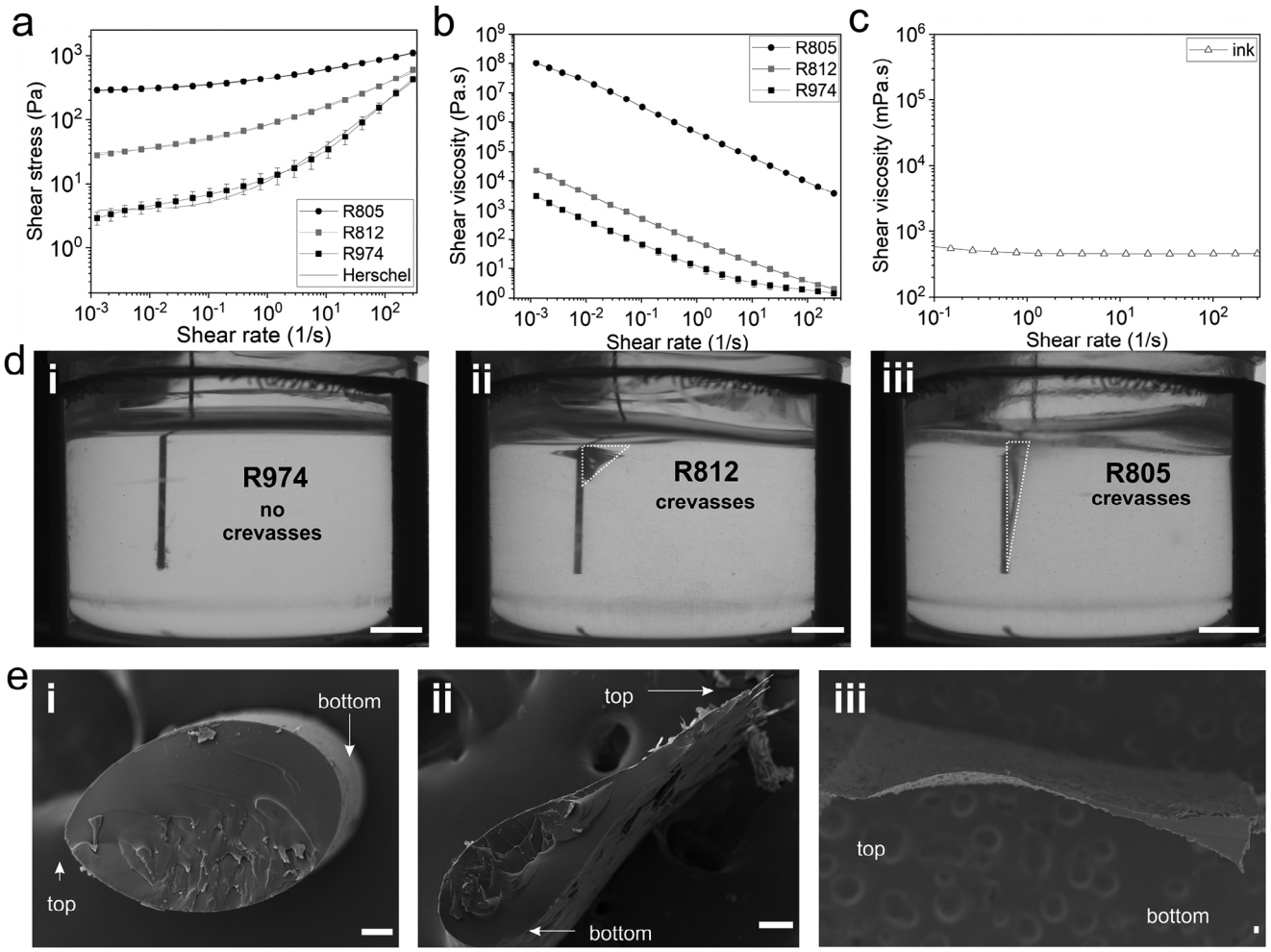

Figure 2. Influence of the yield stress of hydrophobic gels gR974, gR812, and gR805 (fumed silicas in polyethylene glycol (PEG) at 10%w/v) on crevasse formation and on the cross-section of the embedded MD700 printed filaments. a) Analysis of the yield stresses of the supporting baths gels, which are 10 Pa, 37 Pa and 248 Pa for gR974, gR812, and gR805, respectively as determined by Herschel-Bulkley fit. b) Shear shining behavior of the supporting gels: shear-thinning behavior in the range of shear rates exerted by the printing needle (21 s^{-1}) was observed. c) Fluorinated acrylate MD700 ink was tested for its rheological behavior. MD700 ink shows low-viscosity Newtonian behavior. d) Images of the printing needle during printing of ink MD700 at a speed of 15 mm s^{-1} at ≈12 mm depth in supporting baths i) gR974, ii) gR812 and iii) gR805, showing the formation of crevasses of increasing height with increasing yield stresses. Scale bars 5 mm. e) Scanning electron microscopy of the resulting cross-section of the single-filament prints in (d). The filaments retain a rounded cross-section only when printed in the low yield stress supporting bath gR974 (i). With higher yield stresses supporting baths, the formation of crevasses leads to drop-shaped (ii) or elongated line-shaped (iii) filaments. Scale bars 50 µm.

hydrophobic character, immiscibility with PEG and low interfacial tension 0.4 mN m^{-1}. Due to its hydrophobic character the interfacial tension with water is high that makes the material unsuited for printing in classical matrices like, e.g. Carbopol (see Figure S2, Supporting Information). The viscosity of the ink was analyzed, and show Newtonian behavior and a viscosity of 0.45 Pa.s was observed (Figure 2c). The viscosity of the ink is thus lower than the viscosity of the supporting gels at the printing speed, which are 3, 10, and 33 000 Pa.s for gR974, gR812, and gR805, respectively, as shown in Figure 2b. Due to the low viscosity, it is likely that the ink can fill the crevasses, which leads to filament deformation. Single printed filaments were analyzed using SEM (Figure 2e). In R974, with readily collapsing crevasses the ink maintains a rounded cross-section due to the tubular shape of the needle (Figure 2e,i). However, at higher yield stresses of the supporting bath, when static crevasses are present, a low-viscosity ink fills the crevasses immediately leading to a distortion of the ideal filament to a drop-shape for gR812 (Figure 2e,ii) and an elongated line for gR805 (Figure 2e,iii). Thus, a low-yield stress gel like gR974 would be the best choice to achieve uniform, round-shaped filaments and high shape-accuracy prints.

3.1. Adjusting Rheology of Ink to Mitigate Effect of Crevasses

As low-viscosity ink readily flows into crevasses, the rheological modification of the ink should lead to a reduction of this effect. To analyze the effect of the ink rheology on the final shape of the printed filaments, we engineered two inks based on MD700 by introducing fumed silica as a rheological modifier. MD700

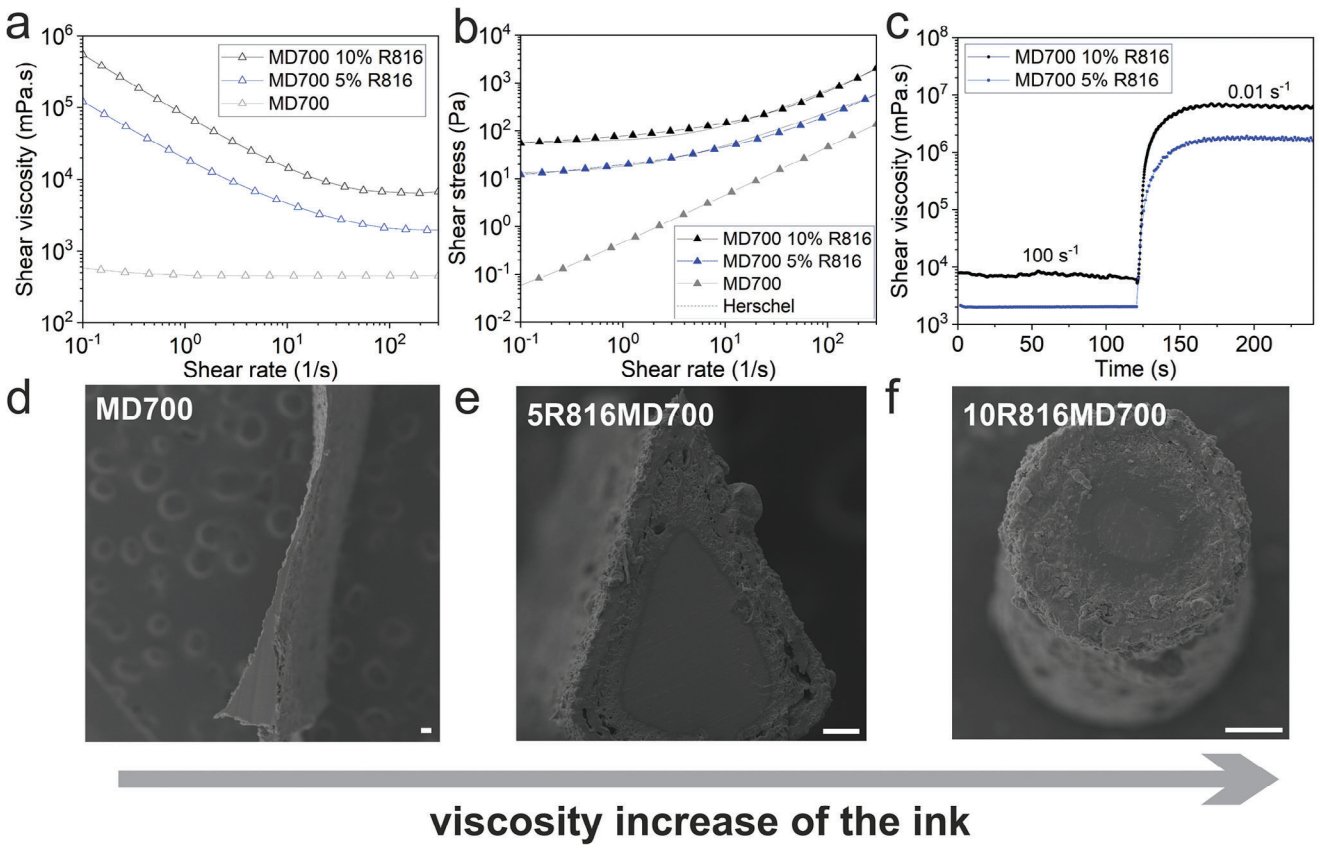

Figure 3. Reducing the effect of crevasses on filament shape by rheological adjustment of the printing ink. The rheology of fluorinated acrylate ink MD700 was adjusted using fumed silica R816 5% (w/v), and 10% (w/v). Resulting inks are denoted as 5R816MD700 and 10R816MD700. The modification leads to a) increased shear viscosity and a shear thinning effect and b) yields stresses of 12 Pa and 56 Pa for 5R816MD700 and 10R816MD700, respectively. c) The shear viscosity of the modified ink with fumed silica R816 10% increase its viscosity faster than the modified ink with fumed silica R816 5% (w/v) after the extrusion rate. Scanning electron microscopy of the cross-section of prints in gR805 from d) unmodified ink MD700, e) MD7000 modified with R816 5% (w/v), and f) MD7000 modified with R816 10% (w/v). Despite the formation of crevasses in gR805, the filaments can be printed with a round cross-section due to the rheological modification of the ink. Scale bar for d, e, f: 50 µm.

was modified with fumed silica R816 by 5% w/v (referred to as 5R816MD700) and 10% w/v (referred to as 10R816MD700). The effect on the rheological properties of the ink was tested. **Figure** 3a shows the shear viscosity of the created inks at the extrusion shear rate, which is in the range of 100–1000 s^{-1}.[35] It can be observed that by the addition of the fumed silica, the viscosity at the extrusion rate 100 s^{-1} increased from 0.45 Pa s without modification to 2 and 6.6 Pa s for 5R816MD700 and 10R816MD700. Additionally, the modification induced a yield stress in the inks, of 12 and 56 Pa for 5R816MD700 and 10R816MD700 (see Figure 3b). The ink behavior upon the sudden change of shear rates was studied to ensure that the viscosity mimics the situation of the extrusion where the ink is sheared at ≈100 s^{-1}[35] and then returns to an unsheared state. Figure 3c indicates that the ink, increases its viscosity (≈0.01 s^{-1}) immediately after the extrusion, leading to a stronger resistance to flow behind the needle for 10R816MD700 than 5R816MD700. The engineered inks were tested for their printing behavior in gR805, which is the supporting bath with the highest yield stress showing crevasse formation (see Figure 2d,iii). In gR805, the filament shape for unmodified MD700 is shown in Figure 3d, showing again the elongated square shape (compare also Figure 2e,iii). With increasing shear viscosity and shear stress, the cross-section of the filament changes from a triangular shape of 5R816MD700 (Figure 3e) to a completely round cross-section for 10R816MD700 (Figure 3f). Thus, printing in a supporting bath that shows crevasse formation is still possible by correct adjustment of the printing ink (see Figure S3, Supporting Information). The frequency sweep test of the modified ink 10R816MD700 shows gel-like behavior at low frequency (see Figure S4, Supporting Information) demonstrating that the ink does not flow easily after being extruded in the supporting bath.

3.2. Combination of Ink and Matrix Rheology for High Accuracy Prints

To achieve a high-accuracy print, besides the overall supporting properties of the baths, the overall stability of the printed shapes is of high importance. Immediately after the needle shears the supporting bath, the bath must re-solidify quickly to trap the printed filaments, keep the shape of the filaments, and allow to print the successive layers of filament without distortion of the previous ones. Thus, it is crucial to determine the recovery time

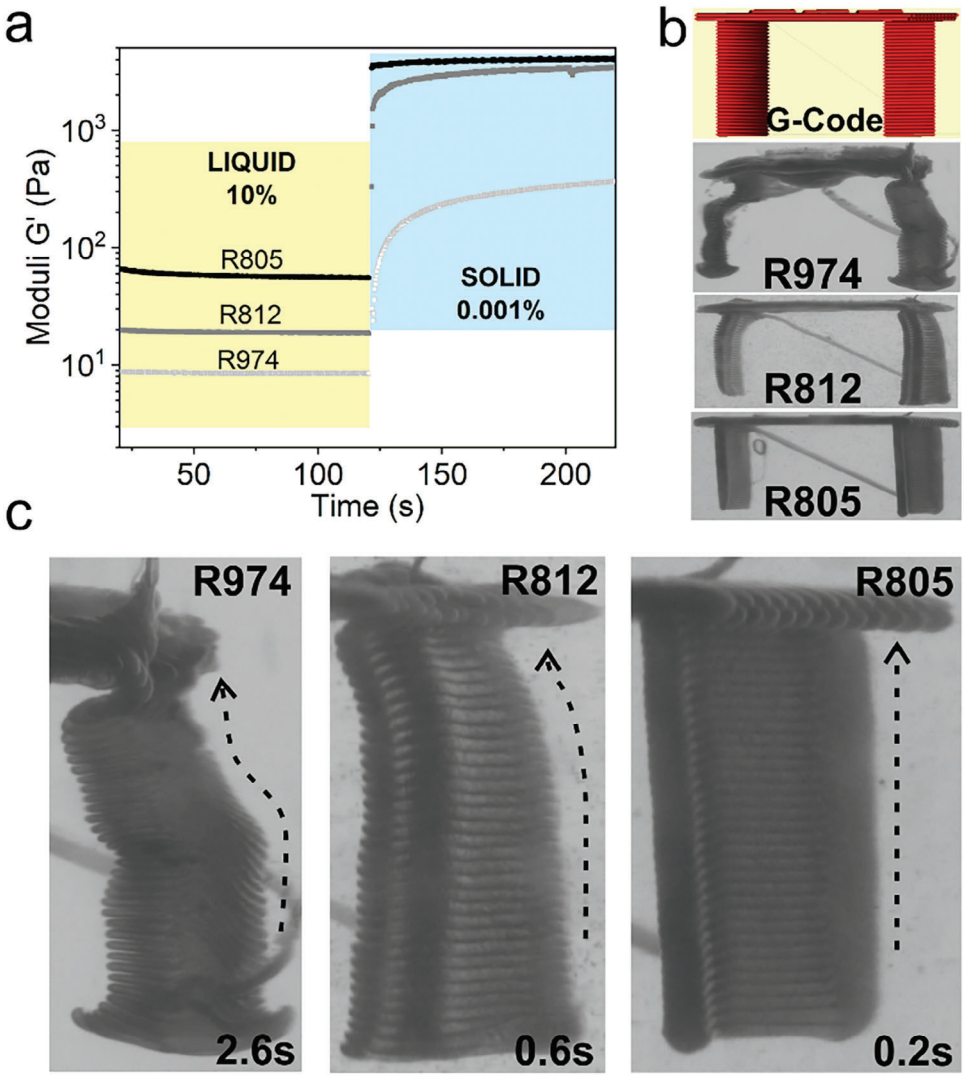

Figure 4. Combination of ink and matrix rheology for high accuracy prints. Recovery time of gR974, gR812, and gR805 and their impact on the accuracy of 3D printing. a) Oscillatory time sweep test to quantify the time needed to achieve 80% recovery of G′ with recovery times of 2.6, 0.6, and 0.2 s for R974, R812, and R805, respectively. b) G-Code model and bridge structures printed into gR974, gR812, and gR805 with optimized ink 10R816MD700 showing the high accuracy prints only for supporting bath gR805 with a fast recovery time of 0.2 s. c) Close-up of the bridge-structures presented in (b), showing the stability and accuracy of the 3D standing structure for optimized ink 10R816MD700 in supporting bath gR805 with fast recovery times.

of the supporting bath. An oscillatory time sweep test was performed to quantify the time that the elastic modulus G′ needs to recover the solid state after high deformation. According to the amplitude sweep test in Figure S1 (Supporting Information), a low strain of 0.001% within the linear viscoelastic region was applied to mimic the rest behavior and a large strain of 10% of the non-linear viscoelastic region was used to guarantee a complete deformation of the network formed by the interactions of the fumed silica particles. **Figure** 4a illustrates the recovery behavior of each gel. The network formed by the dimethylsilyl alkyl chain (R974) interactions required 2.6 s to restor 80% of G′, the trimethylsilyl (R812) reduced this time to 0.66 s, and the highest length of the chain (R805) required the shortest structure recovery time of 0.2 s. To determine how the recovery time plays a major role in the printing accuracy, we used the previously engineered ink 10R816MD700 for printing in the three supporting baths: gR974, gR812, and gR805. A geometrical figure of a bridge was chosen as a test geometry. The results show that the supporting bath with the fastest recovery properties results in the highest accuracy prints (see Figure 4b). In the close-up in Figure 4c, the high accuracy is demonstrated on one of the upward printed features of the bridge, showing that only in gR805 the features of the bridge are correctly printed in a straight manner. The supporting baths gR805 can be re-used as there is no significant change in the supporting properties after shearing (see Figure S5, Supporting Information).

To reduce the recovery time of the supporting bath, the printing speed can also be adjusted. To test whether this adjustment of printing speed would be sufficient to allow for printing in a low-yield stress bath, unmodified MD700 ink and modified ink 10R816MD700 in low-yield stress supporting bath gR974 were printed. The results are shown in Figures S6 and S7 (Supporting

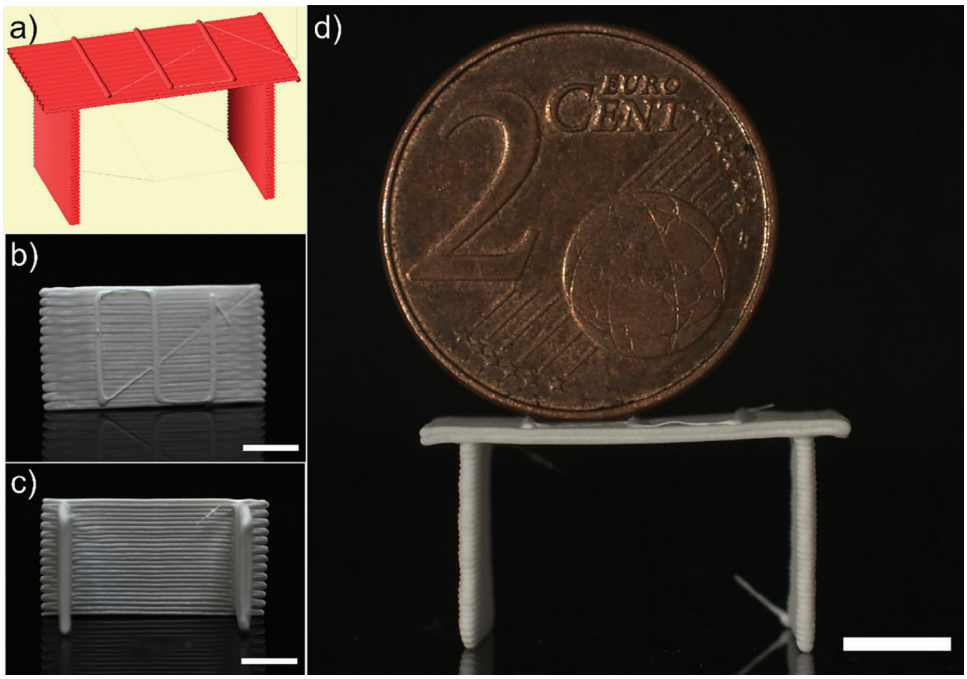

Figure 5. Final 3D-prints after removing the supporting medium. The finished 3D-printed product using 10R816MD700 as ink was removed from the supporting bath gR805. a) The 3D model with three embossments on the top, b) the top view of the final 3D print with the embossments showing the quality of the horizontal filament regardless of the three filaments printed at 90° on the top. c) the bottom view and d) the final bridge showing stability by supporting a weight on the top.

Information). The results show that in general a print can be achieved, but the precision is far from the results shown with 10R816MD700 in the high-yield stress supporting bath gR805 shown in Figure 4. Lower printing speeds are not feasible with our system, but may lead to higher precision prints – at the cost of very high printing times.

The resulting final print is taken from the bath and shown in **Figure 5**. For comparison, a low-viscosity, unmodified MD700 ink was printed in a low-viscosity supporting bath gR974, see Figure S7 (Supporting Information). The results confirm that a faster recovery time of the bath is needed to hold the structure in place as shown by gR805, which requires the modification of the ink.

4. Conclusion

In this paper we showed that by careful engineering of the rheology of printing ink and supporting baths for embedded printing, high accuracy prints can be generated. We prepared yielding fluids gR974, gR812 and gR805 from three differently functionalized fumed silicas in PEG200. We show that in the polar PEG solvent the long alkyl-chain (octylsilyl) on the surface of fumed silica R805 leads to a higher yield stress, a higher viscosity and a faster recovery time of the viscoelastic properties after shearing compared to fused silicas R974 and R812, which contain diemthylsilyl and trimethylsilyl surface groups, respectively. The higher yield stress of the supporting bath is beneficial for holding the ink in place, and the higher yield stress bath gR805 also shows the fastest recovery time. However, the high yield stress of gR805 also leads to crevasse formation, which then leads to the deformation of the printed filament cross-section. We show that by engineering the properties of the printing ink, this effect can be reduced to give well-shaped filaments also in supporting baths with high yield stresses. Our results suggest that high accuracy printing results in embedded printing can be achieved by simple rheological modifications of the system. Our findings will pave the way for more complex embedded prints in various materials.

Supporting Information

Supporting Information is available from the Wiley Online Library or from the author.

Acknowledgements

The work was funded by the Federal Ministry of Education and Research (BMBF) within the program "NanoMatFutur2019", project 03XP029. The authors would like to acknowledge Freiburg Materials Research Center (FMF) and Freiburg Center of Interactive Materials and Bioinspired Technologies (FIT) in University of Freiburg for participation in this study. G.V. acknowledge the financial support of the Secretariat of Higher Education, Science, Technology, and Innovation from the Ecuadorian government (SENESCYT).

Conflict of Interest

The authors declare no conflict of interest.

Data Availability Statement

The data that support the findings of this study are available in the supplementary material of this article.

Keywords

crevasses in embedded printing, embedded 3D-printing, rheology of inks, supporting baths

Received: April 3, 2024
Revised: October 31, 2024
Published online:

[1] T. Bhattacharjee, S. M. Zehnder, K. G. Rowe, S. Jain, R. M. Nixon, W. G. Sawyer, T. E. Angelini, *Sci. Adv.* **2015**, *1*, 1500655.
[2] T. J. Hinton, Q. Jallerat, R. N. Palchesko, J. H. Park, M. S. Grodzicki, H.-J. Shue, M. H. Ramadan, A. R. Hudson, A. W. Feinberg, *Sci. Adv.* **2015**, *1*, 1500758.
[3] N. Chen, *J. Mech. Behavior of Biomed. Mater.* **2023**, *146*, 106083.
[4] T. J. Hinton, A. Hudson, K. Pusch, A. Lee, A. W. Feinberg, *ACS Biomater. Sci. Eng.* **2016**, *2*, 1781.
[5] B. Román-Manso, R. D. Weeks, R. L. Truby, J. A. Lewis, *Adv. Mater.* **2023**, *35*, 2209270.
[6] C. S. O'Bryan, T. Bhattacharjee, S. L. Marshall, W. G Sawyer, T. E. Angelini, *Bioprinting* **2018**, *11*, 00037.
[7] Y. Jin, C. Liu, W. Chai, A. Compaan, Y. Huang, *ACS Appl. Mater. Interfaces* **2017**, *9*, 17456.
[8] J. T. Muth, D. M. Vogt, R. L. Truby, Y. Mengüç, D. B. Kolesky, R. J. Wood, J. A. Lewis, *Adv. Mater.* **2014**, *26*, 6307.
[9] L. Ning, R. Mehta, C. Cao, A. Theus, M. Tomov, N. Zhu, E. R. Weeks, H. Bauser-Heaton, V. Serpooshan, *ACS Appl. Mater. Interfaces* **2020**, *12*, 44563.
[10] F. Jiang, M. Zhou, D. Drummer, *Polymers* **2022**, *14*, 3107.
[11] A. K. Grosskopf, R. L. Truby, H. Kim, A. Perazzo, J. A. Lewis, H. A. Stone, *ACS Appl. Mater. Interfaces* **2018**, *10*, 23353.
[12] S. Duraivel, D. Laurent, D. A. Rajon, G. M. Scheutz, A. M. Shetty, B. S. Sumerlin, S. A. Banks, F. J. Bova, T. E. Angelini, *Science* **2023**, *379*, 1248.
[13] Y. Jin, K. Song, N. Gellermann, Y. Huang, *ACS Appl. Mater. Interfaces* **2019**, *11*, 29207.
[14] Q. Wu, K. Song, D. Zhang, B. Ren, M. Sole-Gras, Y. Huang, J. Yin, *Matter* **2022**, *5*, 3775.
[15] A. Z. Nelson, B. Kundukad, W. K. Wong, S. A. Khan, P. S. Doyle, *Proc. Natl. Acad. Sci., U. S. A.* **2020**, *117*, 5671.
[16] S. Chen, Q. Shi, T. Jang, M. S. B. Ibrahim, J. Deng, G. Ferracci, W. S. Tan, N. Cho, J. Song, *Adv. Funct. Mater.* **2021**, *31*, 2106276.
[17] M. J. Rodriguez, T. A. Dixon, E. Cohen, W. Huang, F. G. Omenetto, D. L. Kaplan, *Acta Biomater.* **2018**, *71*, 379.
[18] Z. Wang, B. Zhang, Q. He, H. Chen, J. Wang, Y. Yao, N. Zhou, W. Cui, *Research* **2023**, *6*, 0122.
[19] H. Kim, J. Kim, K.-H. Ryu, J. Lee, H.-J. Kim, J. Hyun, J. Koo, *ACS Omega* **2023**, *8*, 23554.
[20] A. Z. Nelson, K. S. Schweizer, B. M. Rauzan, R. G. Nuzzo, J. Vermant, R. H. Ewoldt, *Current Opinion in Solid State and Mater. Sci.* **2019**, *23*, 100758.
[21] M. Kawaguchi, *J. Dispersion Sci. Technol.* **2017**, *38*, 642.
[22] S. M. Olhero, J. M. F. Ferreira, *Powder Technol.* **2004**, *139*, 69.
[23] J.-N. Paquien, J. Galy, J.-F. Gérard, A. Pouchelon, *Colloids and Surfaces A: Physicochem. Engineer. Aspects* **2005**, *260*, 165.
[24] Q. Zhang, C. Wu, Y. Song, Q. Zheng, *Polymer* **2018**, *148*, 400.
[25] S. R. Raghavan, H. J. Walls, S. A. Khan, *Langmuir* **2000**, *16*, 7920.
[26] T. G. Maciá-Agulló, J. C. Fernández-García, A. Torró-palau, A. C. Orgilés Barceló, J. M. Martín-Martínez, *The J. Adhesion* **1995**, *50*, 265.
[27] X.-Q. Liu, R.-Y. Bao, X.-J. Wu, W. Yang, B.-H. Xie, M.-B. Yang, *RSC Adv.* **2015**, *5*, 18367.
[28] A. D. Moriana, T. Tian, V. Sencadas, W. Li, *Korea-Aust. Rheol. J.* **2016**, *28*, 197.
[29] P. Alaee, M. Kamkar, M. Arjmand, *Langmuir* **2022**, *38*, 5006.
[30] S. R. Raghavan, J. Hou, G. L. Baker, S. A. Khan, *Langmuir* **2000**, *16*, 1066.
[31] A. Gleadall, *Addit. Manuf.* **2021**, *46*, 102109.
[32] Y.-G. Lee, K. M. Kim, W. I. Cho, J. M. Ko, *Bulletin of the Korean Chem. Soc.* **2013**, *34*, 1795.
[33] W. Michel, *Int. Polymer Sci. Technol.* **2007**, *34*, 1.
[34] R. R. Chauhan, R. P. A. Dullens, K. P. Velikov, D. G. A. L. Aarts, *RSC Adv.* **2017**, *7*, 28780.
[35] H. L Hernandez, J. W. Souza, E. A. Appel, *Macromolecular Biosci.* **2021**, *21*, 2000295.
[36] L. M. Friedrich, J. E. Seppala, *Soft Matter* **2021**, *17*, 8027.